Rapid Communication in Photoscience(2014), vol. 3, no. 1, pp.20-24
http://dx.doi.org/10.5857/RCP.2014.3.1.20

ISSN 2234-8182(Print)
ISSN 2288-4564(Online)

Communication

Sol-Gel Derived Nitrogen-Doped TiO_2 Photoanodes for Highly Efficient Dye-Sensitized Solar Cells

Sang Gyun Kim[§], Myung Jong Ju[§], In Taek Choi, Won Seok Choi, and Hwan Kyu Kim*

Global GET-Future Lab. and Department of Advanced Materials Chemistry, Korea University, 2511 Sejong-ro, Sejong 339-700, Korea

ABSTRACT: N-doped anatase TiO_2 nanoparticles were prepared by the sol-gel process followed by a hydrothermal treatment and successfully used as the photoanodes in organic dye-sensitized solar cells (DSSCs). As expected, the power conversion efficiency (PCE) of 8.44% was obtained for the NKX2677/HC-A-sensitized DSSC based on the 30 mol% N-doped TiO_2 photoanode, which was an improvement of 23% relative to that of the DSSC based on the NKX2677/DCA.

Dye-sensitized solar cells (DSSCs) are promising as an inexpensive alternative to conventional p-n junction solar cells owing to their low cost, simple device fabrication process, and high power conversion efficiency (PCE).[1,2] However, further improving the energy conversion efficiency of DSSCs is important for its successful commercialization. A typical DSSC consists of transparent conducting oxide (TCO), dye-coated nanocrystalline porous oxide (TiO_2), electrolyte, and counter electrode (CE). Attached to the surface of the TiO_2 is a monolayer of the charge transfer dye. The TiO_2 photoanode in DSSCs is one of the most important components, and its role is to act as a support for the dye molecules and as a region for electron transport. In recent years, great progress has been made in TiO_2 doping materials, such as metal doping (Zn-, Ta- and Nb-doping)[3-5] and nonmetal doping (N- and B-doping).[6,7] Of these materials, it has been proved that the N-doping TiO_2 materials can enhance photocurrent and retard electron recombination in DSSCs.

In this work, we have synthesized N-doped anatase TiO_2 nanoparticles by means of the sol-gel process followed by a hydrothermal treatment,[8] and then, conducted a systematic investigation of N-doped TiO_2 electrodes for DSSCs. The sol-gel technology provides an opportunity to prepare nano-sized TiO_2. A series of nanocrystalline N-doped TiO_2 with varying initial N/Ti molar ratios was synthesized. In addition, the optimum N dopant amount for N-doped TiO_2 photoanodes was calculated by Mott-Schottky measurement, and both the charge-transfer behavior and electron lifetime were studied by means of electrochemical impedance spectroscopy (EIS) analysis. The current-photovoltaic (*J-V*) characteristics of the NKX2677/DCA-sensitized DSSCs based on the N-doped TiO_2 with different N-doping amount are shown in **Figure S1**, and the detailed photovoltaic parameters are summarized in **Table S1**. The NKX2677/DCA-sensitized DSSC based on the pure TiO_2 electrode showed a conversion efficiency to be 6.05%. Meanwhile, NKX2677/DCA-sensitized DSSCs based on the N-doped TiO_2 electrodes showed the conversion efficiency to be 6.55 ~ 6.60%. The conversion efficiencies of the DSSCs were slightly enhanced by N-doped TiO_2 electrodes (**Figure S1**). As can be seen in **Figure S1**, the photocurrents of the DSSCs based on the N-doped electrodes gradually increased along with an increase in the N-doping amount. The open circuit voltage (V_{oc}) of the DSSCs increased in the relatively low N-doped TiO_2 photoanode, however, it was decreased after further increase in the N-doping amount.

Figure 1 shows the *J-V* curves and incident photo-current efficiency (IPCE) spectra of the optimized DSSCs, and their detailed photovoltaic parameters were summarized in **Table 1**. The NKX2677/DCA-sensitized DSSC based on the N30 TiO_2 (D3) exhibited an efficiency of 6.86%. Meanwhile, the NKX2677/DCA-sensitized DSSC based on the pure TiO_2 (D2) exhibited an efficiency of only 6.05%. The conversion efficiency of the DSSC was slightly increased by N-doped TiO_2 electrode. The efficiency of the NKX2677/HC-A-sensitized DSSC could be further increased by a multi-functional

***To whom correspondence should be addressed.**
E-mail: hkk777@korea.ac.kr

coadsorbent HC-A,[9] instead of a DCA. The conversion efficiency of the NKX2677/HC-A-sensitized DSSC based on the N30 TiO_2 (D4) was significantly increased up to 8.44%, which is much higher than that of the NKX2677-sensitized DSSC based on the pure TiO_2 (5.07%) (D1). Moreover, a short-circuit current density (J_{sc}, 15.25 mA/cm^2) and an V_{oc} (0.73 V) of the NKX2677/HC-A-sensitized DSSC based on the N30 TiO_2 photoanode was significantly higher than those of other DSSCs, although the dye adsorbed amount is relatively lower than the others. Also, as can be seen in the NKX2677/HC-A-sensitized DSSCs based on the N30 TiO_2, both a J_{sc} and a V_{oc} are significantly increased in N-doped TiO_2. As shown in Figure 1b, the IPCE spectra exhibited a significant enhancement in the DSSC performance based on the N-doped TiO_2 compared to those of the DSSCs based on the undoped TiO_2 Thus, we can conclude that the intrinsic increase in the photocurrent is primarily related to the enhanced electron injection and transfer ability of the N-doped TiO_2.

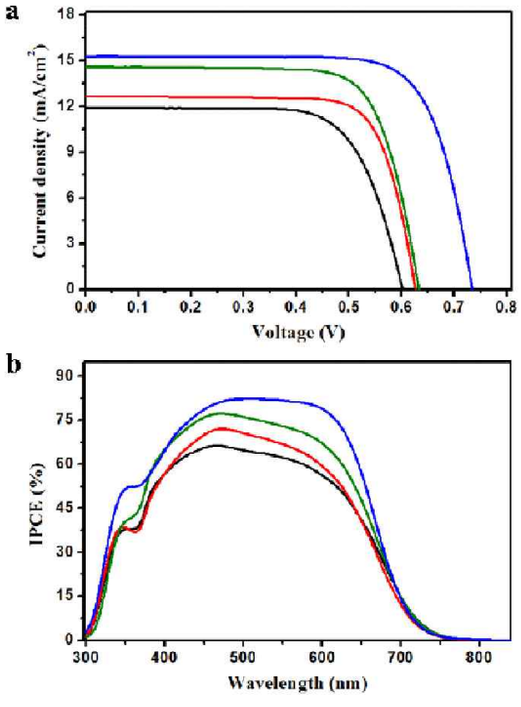

Figure 1. (a) J–V curves of the DSSCs based on pure TiO_2 and N-doped TiO_2 photoanodes. (b) IPCE spectra of the same devices. Pure TiO_2 (NKX2677; D1, black line); pure TiO_2 (NKX2677/DCA; D2, red line); N30 TiO_2 (NKX2677/DCA; D3, green line); N30 TiO_2 (NKX2677/HC-A; D4, blue line). TiO_2 thickness and active area are 12 (8+4) μm and 0.16 cm^2, respectively.

Table 1. Performance Characteristics of the DSSCs Based on the Pure TiO_2 and N30 TiO_2 Photoanodes

Device	Dye absorbed amount (×10^{8}mol/cm^2)	J_{sc} (mA/cm^2)	V_{oc} (V)	FF (%)	PCE (%)
D1	7.5	11.88	0.60	70.9	5.07
D2	4.6	12.65	0.62	76.3	6.05
D3	6.3	14.58	0.63	74.4	6.86
D4	4.2	15.25	0.73	75.3	8.44

UV-vis spectra with respect to the molar ratios of N-doped TiO_2 are shown in **Figure 2**. Nitrogen was doped successfully into TiO_2, since the N-doped TiO_2 photoanodes exhibits the broad visible light absorption. Giamello *et al*[10] reported that the N-doped TiO_2 electrodes contained N centers were responsible for visible light absorption. The N centers consisted of single-atom nitrogen impurities that formed either diamagnetic (N^-) or paramagnetic (N^{*-}) bulk centers.

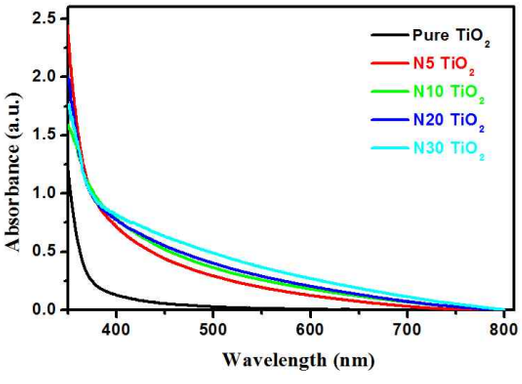

Figure 2. UV-vis spectra of pure TiO_2 and the N-doped TiO_2 powders varied molar ratios N-doping amount.

In order to find out the reasons leading to a higher V_{oc} for the DSSCs based on the N-doped TiO_2, flat-band potential (V_{fb}) measurements of the N-doped and pure TiO_2 electrodes were carried out by means of Mott-Schottky analyses of the impedance spectra,[11] which has been demonstrated to offer significant advantage for determination of the V_{fb} of the semiconductor electrodes.[12] The N20 and N30 TiO_2 electrodes exhibited a negative shift of V_{fb} compared to that of the pure one (Figure 3). On the other hand, V_{oc} is defined as the voltage difference between the electrolyte redox potential (E_{redox}/q) and the quasi-Fermi potential of electrons ($E_{F,n}$/q) in the TiO_2 semiconductor.[13] Considering that redox potential of I^-/I_3^- (E_{red}) would not change strongly in DSSCs fabricated under similar conditions, V_{oc} is determined

by the potential of the conduction band edge (CB) and the electron density (n) in TiO_2. These two parameters are closely related to the surface charge and charge recombination, respectively. Possible factors influencing V_{oc} for DSSCs involve the TiO_2 surface blocking, conduction band movement, and interaction between electrolyte and sensitizer. Therefore, the V_{oc} of the DSSC based on the N-doped TiO_2 increased compared to that of the pure TiO_2 because of the negative shift in V_{fb}. Furthermore, the V_{oc} was further increased in the DSSC based on the N-doped TiO_2, due to the prevention of recombination. using a multi-functional HC-A as a coadsorbent (**Figure 1a**).[9] The HC-A has multiple functions, such as the light-harvesting effect as a short wavelength light absorption dye molecule to increase J_{sc} and the prevention effect of the π–π stacking of organic dye, associated with the hole-conducting function, which enhances V_{oc} by reducing the charge recombination process.

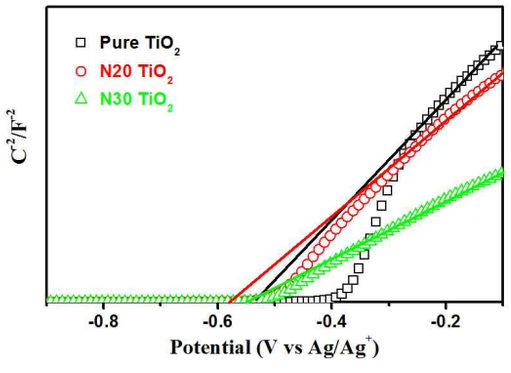

Figure 3. Mott-Schottky plots for the undoped TiO_2 and N-doped TiO_2 films.

The crystal phase identification of N-doped TiO_2 samples was carried out by use of X-ray diffraction (XRD). **Figure 4a** shows the XRD patterns of the pure and N30 TiO_2 powders. All peaks of the TiO_2 samples can be assigned to the anatase phase, indicating that the anatase nanocrystalline structure is retained after N doping, which is consistent with the proposition that the increase in the N-doping content in the TiO_2 lattice enhances the growth of anatase phase TiO_2 and hinders the formation of rutile phase TiO_2. The scanning electron microscopy (SEM) images of the pure and N30 TiO_2 electrodes are shown Figure 4b. These electrodes show dense structure without any cracks. The crystallite sizes of the anatase phase decreased from ca. 24 − 26 to ca. 22 − 24 nm with increasing doping concentration for N-doped TiO_2 samples.

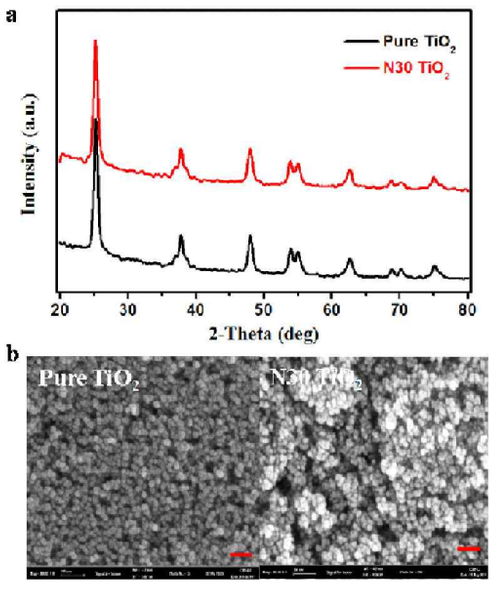

Figure 4. (a) XRD patterns of pure TiO_2 and N30 TiO2 powders. (b) SEM images of pure TiO_2 and N30 TiO_2 powders. Scale bars are 100 nm.

To investigate the difference between N-doped and pure TiO_2 DSSCs with respect to their charge transfer and recombination properties, EIS was performed at open circuit voltage under dark condition. Nyquist and Bode plots of the DSSCs based on the N-doped and pure TiO_2 photoanodes were shown in **Figure S2**. The photovoltaic performance depends strongly on the charge collection efficiency (η_{cc}) derived from $\eta_{cc}=(1+R_t/R_{ct})^{-}1$ or $\eta cc=(1+\tau_t/\tau_r)^{-1}$.[14,15] **Table 2** summarizes the result of the EIS analysis fitted using an equivalent circuit known as the transmission line model,[16] as shown in **Figure 5c**, while fitted Nyquist plots are shown in **Figure 5a** and Nyquist plots at the highest frequency regions are shown in **Figure 5b**. The NKX2677/HC-A-sensitized DSSC based on the N30 TiO_2, exhibited faster electron transport times ($\tau_t=C\mu \cdot R_t$)[16,17] than the DSSCs based on the pure TiO_2. Moreover, its electron lifetime ($\tau_r=C\mu \cdot R_r$)[16,17] was significantly increased, which might also be due to the significant increase in capacitance ($C\mu$) at the interface of the CE/electrolyte solution (**Table 2**). Eventually, the charge collection efficiency of the NKX2677/HC-A-sensitized DSSC based on the N30 TiO_2 reached up to 94% and could demonstrate greatly improved device performance. The EIS results also confirm the mechanism of improvement in the DSSCs based on the N30 TiO_2. Eventually, the charge collection efficiency of the NKX2677/HC-A-sensitized DSSC based on the N30 TiO_2 reached up to 94% and could demonstrate greatly improved device

performance. The EIS results also confirm the mechanism of improvement in the DSSCs based on the N30 TiO_2. The maximum frequencies (ω_{max}) in the middle frequency region of the Bode plots of the NKX2677/HC-A-sensitized DSSCs based on the N30 TiO_2 and pure TiO_2 were 3.1 and 10.5 Hz, respectively (**Figure S2b**). Since ω_{max} is inversely associated with electron lifetime (τ), $\tau=1/(2\pi f)$,[18,19] a decrease in ω_{max} indicates a reduced rate of the charge-recombination process of the DSSCs. The insulating molecular layer of HC-A effectively inhibits back electron transfer from the TiO_2 to I_3^- ions and prevents the V_{oc} drop in the NKX2677/HCA-sensitized DSSC based on the N30 TiO_2.

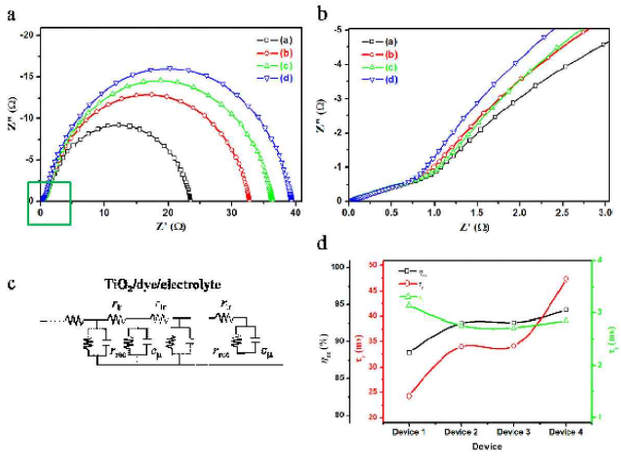

Figure 5. (a) Fitted Nyquist plots from the EIS spectra of the DSSCs at middle frequency region (shown in **Figure S2**), (b) Nyquist plots at the higher frequency regions in **Figure 4a**, (c) the equivalent circuit diagram to calculate the charge transport and recombination resistance and (d) charge collection efficiency, life time and transport time verses different devices. (a) Pure TiO_2 (NKX2677); (b) pure TiO_2 (NKX2677/DCA); (c) N30-doped TiO_2 (NKX2677/DCA); (d) N30-doped TiO_2 (NKX2677/HC-A).

Table 2. Charge Collection Efficiencies Calculated from the EIS Parameters for the DSSCs Based on Pure TiO_2 and N30 TiO_2 Photoanodes

Device	Rt (Ω)	Rct (Ω)	Cμ (mF)	τ_t (ms)	τ_r (ms)	η_{cc} (%)
D1	2.91	22.5	1.08	3.14	24.30	88.5
D2	2.88	35.4	0.96	2.76	33.98	92.5
D3	2.54	31.9	1.07	2.72	34.13	92.6
D4	2.32	38.5	1.23	2.85	47.36	94.3

In summary, N-doped TiO_2 nanocrystalline powders were obtained by employing the sol–gel process, and they were successfully applied as photoanode materials in organic DSSCs. After N doping, anatase TiO_2 structure was retained. The CB of the N doped TiO_2 photoanode was higher than that of the pure TiO_2. On the other hand, the V_{oc} in the DSSCs based on the N doped TiO_2 could be further increased using a multi-functional HC-A as a coadsorbent instead of DCA. As expected, a PCE of 8.44% was obtained for the NKX2677/HC-A-sensitized DSSC based on the N30 TiO_2, which was an improvement of 23% compared with that of the pure TiO_2 counterpart. The improvement was ascribed to the enhanced electron injection and transport efficiency caused by the negative shift in CB of N-doped TiO_2, and the mechanism was verified by EIS analysis.

KEYWORDS: dye-sensitized solar cell, photoanode, TiO_2, N-dopedphotoanode

Received March 14, 2014; Accepted March 24, 2014

ACKNOWLEDGEMENT

This work was supported by the Converging Research Center Program through the Ministry of Science, ICT and Future Planning, Korea (2013K000203). [§]These authors contributed equally to this work.

SUPPORTING INFORMATION

Experimental procedures; synthetic; *J-V* curves; EIS data. This material is available free of charge via the Internet at http://www.rcp.or.kr

REFERENCES AND NOTES

1. O'Regan B.; Grätzel M. Nature **1991,** *353,* 737-740.
2. Grätzel, M. Nature **2001,** *414,* 338-344.
3. Wang, K.-P.; Teng, H. Phys. Chem. Chem. Phys. **2009,** *11,* 9489-9496.
4. Liu, J.; Yang, H.; Tan, W.; Zhou, X.; Lin, Y. Electrochim. Acta **2010,** *56,* 396-400.
5. Kim, S. G.; Ju, M. J.; Choi, I. T.; Choi, W. S.; Choi, H.-J.; Baek, J.-B.; Kim, H. K. RSC Adv. **2013,** *3,* 16380-16386.
6. Tang, J.; Cowan, A. J.; Durrent, J. R.; Klug, D. R.; J. Phys. Chem. C **2011,** *115,* 3143-3150.
7. Tian, H.; Hu, L.; Li, W.; Sheng, J.; Xu, S.; Dai, S. J. Mater. Chem. **2011,** *21,* 7074-7077.
8. Cong, Y.; Zhang, J. L.; Chen, F.; Anpo, M. J. Phys. Chem. C **2007,** *111,* 10618-10623.
9. Song. B. J.; Song, H. M.; Choi, I. T.; Kim, S. K.; Kang D. S; Kang, M. S.; Lee, M. J.; Cho, D. W.;

Ju, M. J.; Kim, H. K. Chem. Euro. J. **2011,** *17,* 11115-11121.
10. Valentin, C. D.; Finazzi, E.; Pacchioni, G.; Selloni, A.; Livraghi, S.; Czoska, A. M.; Paganini, M. C.; Giamello, E. Chem. Mater. **2008,** *20,* 3706-3714.
11. Munoz, A. G.; Chen, Q.; Schmuki, P. J. Solid State Electrochem. **2007,** *11,* 1077-1084.
12. Nagasubramanian, G.; Wheeler, B. L.; Fu-Ren, F. F.; Allen. J. B. J. ElectroChem. Soc. **2007,** *129,* 1742-1745.
13. Green, M. A.; Solar Cells: Operating Principles, Technology, and System Applications, Prentice-Hall, Englewood Cliffs, NJ, **1982.**
14. Schlichthörl, G.; Park, N. G.; Frank, A. J. J. Phys. Chem. B **1999,** *103,* 782−791.
15. Van de Lagemaat, J.; Park. N. G.; Frank. A. J. J. Phys. Chem. B **2000,** *104,* 2044−2052.
16. Bisquert, J.; Fabregat-Santiago, F.; Mora-Sero, I.; Garcia-Belmonte, G.; Gimenez, S. J. Phys. Chem. C **2009,** *113,* 17278-17290.
17. Nissfolk, J.; Fredin, K.; Hagfeldt, A.; Boschloo, G. J. Phys. Chem. B **2006,** *110,* 17715-17718.
18. ang, Q.; Zhang, Z.; Zakeeruddin, S. M.; Grätzel, M. J.Phys. Chem. C **2008,** *112,* 7084-7092.
19. Kern, R.; Sastrawan, R.; Ferber, J.; Stangl, R.; Luther, J. Electrochim. Acta **2002,** *47,* 4213 −4225